Dalton Transactions

ROYAL SOCIETY OF CHEMISTRY

COMMUNICATION

View Article Online
View Journal | View Issue

Cite this: *Dalton Trans.*, 2023, **52**, 15326

Received 4th May 2023,
Accepted 9th June 2023

DOI: 10.1039/d3dt01325a

rsc.li/dalton

Dipotassiumtetrachloride-bridged dysprosium metallocenes: a single-molecule magnet†

Selvakumar Arumugam,[a] Björn Schwarz, *[b] Prathap Ravichandran,[a] Sunil Kumar, [a] Liviu Ungur *[c] and Kartik Chandra Mondal *[a]

The present work describes the dynamic magnetic properties of the complex $[(Cp^{Ar3})_4Dy^{III}_2Cl_4K_2]\cdot 3.5(C_7H_8)$ (1), synthesized by employing a tri-aryl-substituted cyclopentadienyl ligand (Cp^{Ar3}), [4,4′-(4-phenylcyclopenta-1,3-diene-1,2-diyl)bis(methylbenzene) = $Cp^{Ar3}H$]. Each Dy(III)-metallocene weakly couples *via* K_2Cl_4, displaying slow relaxation of magnetization below 14.5 K under zero applied dc field *via* KD3 energy levels with an energy barrier of 136.9/133.7 cm^{-1} on the Dy sites. The single-ion axial anisotropy energy barrier is reduced by geometrical distortion due to the coordination of two chloride ions at each Dy centre.

The coordination chemistry of lanthanides has received much attention due to its applications in catalysis, luminescence and magnetism.[1–5] A special attention has been devoted to molecular magnetism. Single-molecule magnets (SMMs) have the potential to miniaturize storage devices and cause a second quantum revolution. For instance, observation of magnetic hysteresis in certain SMMs with sufficiently high coercivity has inspired analogies between molecular nanomagnets and classical magnets, suggesting that these SMMs can be incorporated into information storage devices. In this regard, cyclopentadienyl-stabilized dysprosium complexes have shown the most promising properties, exhibiting high temperatures and energy barriers for slow relaxation of spin/magnetization. Crystal field engineering, by choosing a suitable ligand system, is one of the most important considerations while designing a SMM. Therefore, a wide range of ligand systems have been utilized since the observation of the SMM property in $[Mn_{12}O_{12}(OAc)_{16}(H_2O)_4]\cdot 2AcOH\cdot 4H_2O$ (Mn_{12}–OAc) in 1991.[6] Among all the ligands tried, cyclopentadienyl ligands have produced the best performing SMMs in terms of blocking temperature and effective energy barriers for slow relaxation of magnetization since they can provide stronger crystal field splitting with the axial approach for coordination.[7] For example, Layfield *et al.* reported a cyclopentadienyl ligand-stabilized dysprosium metallocene cation that exhibits magnetic hysteresis up to 80 K, revealing an effective energy barrier of 1541 cm^{-1}.[7] Additionally, they have further given experimental and theoretical proof that the cyclobutadienyl ligand in dysprosium metallocene could cause stronger crystal field splitting than the cyclopentadienyl ligand.[7–9] A point to be noted is that several classic examples of organometallic ferrocene type sandwich complexes exist in the literature,[10] including lanthanide metallocenes reported in 1956.[11] They have found a wide range of applications;[12] however, they were not studied by dynamic magnetic susceptibility measurements until the last decade. Recently, cyclopentadienyl ligands have significantly contributed to the remarkable progress of SMMs,[7–9] especially bulky alkyl-substituted cyclopentadienyl ligands.[13] The reason behind using bulky substituted cyclopentadienyl ligands is their ability to stabilize Dy^{3+}, which can significantly enhance the axiality of their crystal field.[14] For instance, in monometallic Dy^{3+} sandwich complexes, more bulky Cp groups cause larger Cp–Dy–Cp angles and short Cp_{cent}–Dy distances leading to increased effective energy barriers and blocking temperatures.[7–9] The magneto-structural correlations suggest that a striking balance exists between Dy–Cp distances and Cp–Dy–Cp bond angles and this is a vital consideration. While trying to achieve the highest possible axial geometry with the help of bulky substituted cyclopentadienyl ligands, it should be kept in mind that the ligands should reach proximity to the metal ion so that the large crystal field splitting of Kramers doublets (KDs) can be achieved. Recently, lanthanide chemistry has also witnessed the development of bifunctional materials such as magneto-luminescent materials[15] that can be employed in various applications, including data storage devices,[16] quantum computing,[17] light-emitting diodes[18] and fluorescence labeling.[19] Poly-aryl-substituted cyclopentadienyl ligands have been used to synthesize luminescent lanthanoid

[a]*Department of Chemistry, Indian Institute of Technology Madras, Chennai, India. E-mail: csdkartik@iitm.ac.in*
[b]*Institute for Applied Materials – Energy Storage Systems (IAM-ESS), Karlsruhe Institute of Technology (KIT), Hermann-von-Helmholtz-Platz 1, 76344 Eggenstein-Leopoldshafen, Germany. E-mail: bjoern.schwarz@kit.edu*
[c]*Department of Chemistry, National University of Singapore, Singapore. E-mail: chmlu@nus.edu.sg*

†Electronic supplementary information (ESI) available. See DOI: https://doi.org/10.1039/d3dt01325a

compounds with excellent magnetic properties.[20–23] Layfield, Winpenny *et al.* have reported mono- and dichloride-bridged zig-zag-chain (**A**), discrete dimeric-unit (**B**) and THF-coordinated discrete dimeric-unit (**C**) Dy-metallocenes (Scheme 1).[21f] Several Dy-metallocene-containing systems have been extensively studied in the last decade.[21–29d] Other structurally similar analogs of **A**–**C** are mono-cationic monomeric units **D** and **E**, which have been recently reported by Demir *et al.*[29a] Very recently, a $(Cl–K–Cl)_2$ bridged tetrameric Dy(III) complex (**F**) has been reported by Gao *et al.*[29b] It has been observed that aryl-bonded (**G**) and aryl-bridged (**H**) Dy-metallocenes display much better SIM/SMM properties.[22b,29c] A $N_2^{3\bullet-}$ bridged dinuclear Dy(III)-metallocene showed increased axial magnetic anisotropy leading to its blocking temperature (U_{eff} = 108 cm^{-1}; $J_{Dy–rad}$ = −7.2 cm^{-1}).[29d] Dinuclear Dy(III) complexes having two μ-O bridges with asymmetric auxiliary ligands showed improvement in their SMM behavior.[29e] The steps in their hysteresis loops can be further controlled by introducing chloride bridges.[29f] Herein, we report a detailed study of the magnetic properties of a K_2Cl_4-bridged dimeric dysprosium metallocene compound, $[(Cp^{Ar3})_4Dy^{III}_2Cl_4K_2]·3.5(C_7H_8)$ (**1**), the synthesis and luminescence properties of which have been reported previously.[24]

Light yellow blocks of $[(Cp^{Ar3})_4Dy^{III}_2Cl_4K_2]·3(C_7H_8)$ (**1**) were isolated from a concentrated toluene solution when anhydrous $DyCl_3$, $Cp^{Ar3}H$ and potassium were reacted in a 1 : 2 : 2 molar ratio at 110 °C for two days (Scheme 2).[24] The relevant Dy complexes are shown in Scheme 1.

The complex $[(Cp^{Ar3})_4Dy^{III}_2Cl_4K_2]·3.5(C_7H_8)$ (**1**) does not possess a center of inversion within the molecular unit of **1**, although it crystallizes in the triclinic $P\bar{1}$ space group.[24] The core of the complex, $Dy_2K_2Cl_4$, exhibits a butterfly-like shape wherein Cl^- ions are present as bridging anions connecting Dy^{3+} and K^+ ions (Fig. 1). Two different $(Cp^{Ar3})_2Dy^{III}$ units are separated by a K_2Cl_4 unit in the middle of the core. Two Dy^{3+} ions occupy the wing positions, while K^+ ions are there for charge balance preferring body positions. Each K^+ ion is sandwiched between two η^6-phenyl rings (Dip) in a bent fashion with K–C distance of 3.0729(12)–3.502(3) Å. Each Dy^{3+} ion is

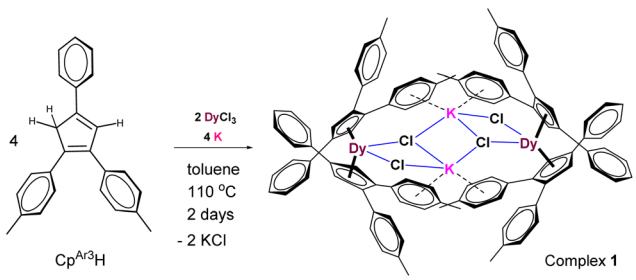

Scheme 2 Synthesis of the complex $[(Cp^{Ar3})_4Dy^{III}_2Cl_4K_2]·3.5(C_7H_8)$ (**1**).

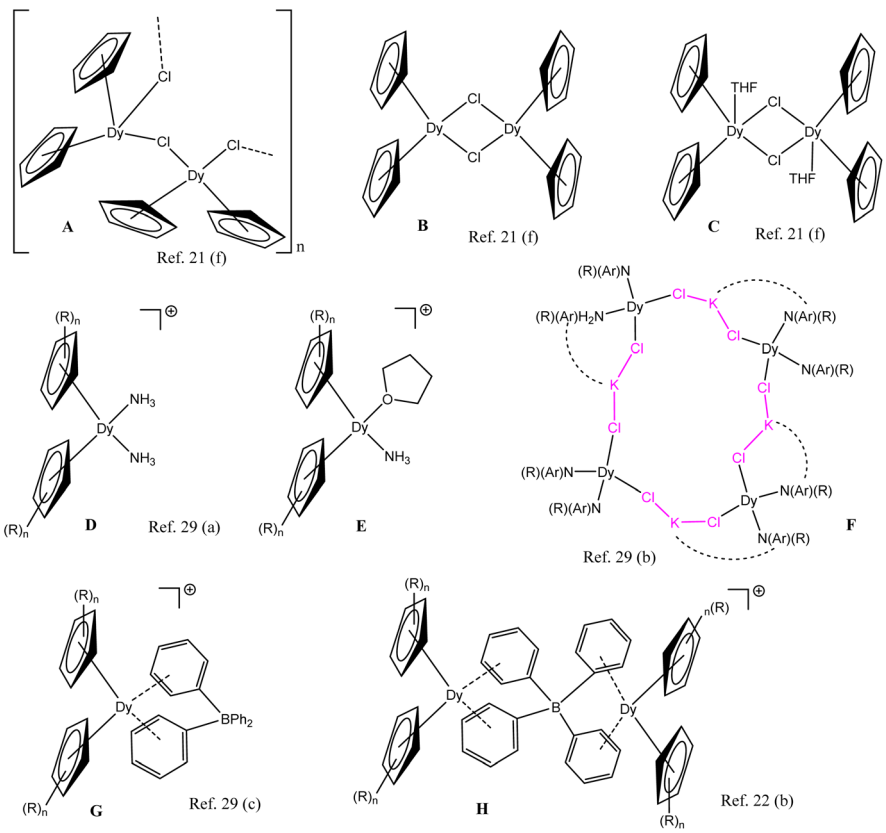

Scheme 1 Previously reported relevant Cp–Dy complexes.

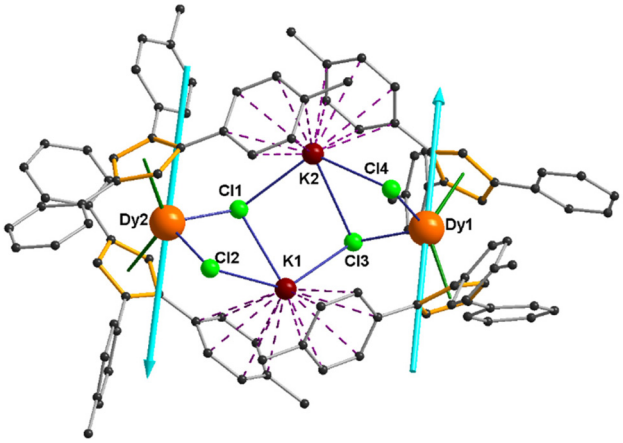

Fig. 1 Molecular structure of complex **1**. The hydrogen atoms are omitted for clarity. Selected bond lengths (Å) and bond angles (°) are as follows: Dy2–Cl1 2.6185(8), Dy2–Cl2 2.5874(8), Dy1–Cl3 2.5993(8), Dy1–Cl4 2.5903(8); Dy2–Cl1–K2 129.24 (3), Dy2–Cl1–K1 97.95 (3). The cyan arrows represent the axis of magnetic anisotropy. Orientation of local magnetic axes (g_Z) in the ground Kramers doublets of the individual Dy sites of **1** together with the orientation of the local magnetic moments in the ground exchange state.

sandwiched between two η^5-cyclopentadienyl rings with Dy–C distances ranging from 2.644(3) to 2.768(3) Å, which are close to the values (2.606(6)–2.647(7)/2.638(12)–2.706(12) Å; **B**/**C**) reported for **A**–**C**, which contain one type of Dy centre.[21f] The sandwiched Dy^{3+} ions form a dinuclear bent metallocene ultimately with the coordination of two Cl^- anions at each Dy^{3+} ion. The axial orientations of the two Cp rings of each Dy ion of **1** are lost due to further coordination by two chloride ions connected to the nearest K^+ ions forming μ and μ_3 bridges. The Cp–Dy–Cp bond angle (centroid of each Cp) of this dinuclear bent Dy-metallocene (**1**) is in the range of 129.73–130.85(5)°. The selected bond length and angle are given in Table S4.† The Cl–Dy–Cl angles of **1** are 87.19/91.63°, which are broader than those of **A**/**B** (89.82/83.38°), while the corresponding value is much higher for **F** (109.03°) and its related chain/other complexes (107.4/106.27°).[29b] The angle between two planes containing the Cp rings is 53.70/52.48°, slightly higher than that of **B** (50.02°).[21f] The intramolecular Dy–Dy distance of **1** is 8.23 Å, which is more than twice that of **B** (4.01 Å), but it is smaller than that of **F** and its other analogs (8.92/10.27/9.0 Å).[29b]

Methods

See the ESI† for synthesis, CV and magnetic measurements.

Ab initio calculations

To acquire additional insight into the electronic structure and magnetic properties of complex **1**, we have employed standard *ab initio* calculations based on multiconfigurational methods, which were done with OpenMolcas software.[30,31] We have used the entire molecular structure for the calculations, as obtained from X-ray analysis. All atoms were described with the ANO-RCC basis sets, which include relativistic corrections for core orbitals. Dy and all closely spaced atoms were described with large VTZP basis sets, while distant atoms were described with medium VDZP basis.[32] All molecular orbitals and low-lying excitation were evaluated with Complete Active Space Self Consistent Field (CASSCF) calculations.[33] The active space of the CASSCF method included the $4f^9$ configuration (CAS(9,7)). All states of the possible spin states (S = 5/2, 3/2, 1/2) were optimized in three different state-averaged CASSCF calculations. The spin–orbit coupling using the atomic mean field integral (AMFI) approximation in the Restricted Active Space State Interaction (RASSI) method further mixed a subset of the optimized states.[34] The resulting spin–orbit eigen states were further used to describe the magnetic properties using the SINGLE_ANISO code.[35–39] This method has been employed many times before, and the results seem reliable since many recent advances in this domain helped in obtaining better single-molecule magnets.[7–14,20–24,28,29] Table 1 shows the obtained fitting parameters of the relaxation *vs.* temperature plots according to two alternative models (eqn (1) and (2)). Table 2 shows the low-lying local energy spectra obtained on individual Dy sites alongside the main values of the *g*-tensor on the ground Kramers doublets. Fig. 1 shows the orientation of the main anisotropy axes in the ground state on individual Dy sites and the direction of the local magnetic moments in the ground exchange state.

Table 1 Obtained fitting parameters of the relaxation *vs.* temperature plots according to two alternative models

Model (1) (QTM + Raman)	
τ_{QTM} (s)	$10^{-3.8(2)}$
C (s^{-1} K^{-n})	$10^{-4(6)}$
n	7(5)
Model (2) (QTM + Orbach)	
τ_{QTM} (s)	$10^{-3.8(2)}$
τ_0 (s)	$10^{-7(2)}$
U_{eff} (K)	100 (70)

Table 2 Low-lying CASSCF/RASSI spin–orbit energy spectra of individual sites in compound **1**

	Dy1		Dy2	
KD	Energy (cm^{-1})	*g*-Tensor	Energy (cm^{-1})	*g*-Tensor
1	0.0	0.0156	0.0	0.0036
		0.0254		0.0045
		18.8117		18.8067
2	72.0	0.1197	78.1	0.0445
		0.1387		0.0671
		16.7179		16.5731
3	136.9	0.3578	133.7	0.0352
		1.0841		0.1843
		17.3824		19.1310
4	174.3	2.5382	204.4	2.4786
		4.1966		4.5318
		11.5138		12.2879
5	193.2		219.2	
6	225.8		252.1	
7	262.1		299.8	
8	365.2		441.5	

Magnetic properties

The theoretical $\chi_M T$ value of **1** for two free Dy^{III} ions of 28.34 cm^3 K mol^{-1} matches the experimentally determined value for complex **1** at 300 K of 28.14 cm^3 K mol^{-1} (Fig. 2).[21f,25,29a]

The weak antiferromagnetic exchange has reduced influence on the magnetic behavior. The field-dependent magnetization at low temperatures rapidly increases in a DC field of up to 10 kOe and, after that, rises steadily in fields up to 70 kOe and achieves its maximum values of 11.18 μ_B at 2 K, 11.11 μ_B at 3 K and 11.12 μ_B at 4 K (Fig. 2). The magnetization at 70 kOe is not saturated and can be attributed to this system's low-lying excited states and/or anisotropy.[21f,26,29] As inferred from the fit to the dc magnetic data, the local magnetic anisotropies cause slow magnetic relaxation, further characterized by ac susceptibility measurements. The slow relaxation of magnetization is evident from the peaks in the out-of-phase susceptibility *versus* frequency plots (χ''_M *vs.* f) (Fig. 3). AC susceptibility *vs.* frequency at different applied DC fields of H = 0 to 2500 Oe has been measured (Fig. S1†). The magnitude of AC susceptibility decreases with increasing DC field. Fig. S2† presents ac susceptibility *vs.* frequency scans and Cole–Cole plots for the selected temperature range of 2 K to 16.5 K (H = 0) to extract the relaxation time parameters for complex **1**. These curves were fitted by a generalized Debye model with parameter α that describes the distribution of relaxation times within the generalized Debye mode, isothermal susceptibility χ_s (at the low-frequency limit where $\omega \ll \tau^{-1}$), χ_t (at the high-frequency limit where $\omega \gg \tau^{-1}$) and the extracted relaxation times τ are listed in Table S1–2.† The extracted inverse relaxation times τ^{-1} *vs.* temperature (shown in Fig. 4) could be fitted with equal quality by two alternative models.

Model (1) consists of a quantum tunneling term (QTM) and a Raman term:

$$\tau^{-1} = {\tau_{QTM}}^{-1} + CT^n, \quad (1)$$

with Raman constant C, temperature T and Raman temperature exponent n. Model (2) consists of a QTM term and an Orbach term:

$$\tau^{-1} = {\tau_{QTM}}^{-1} + {\tau_0}^{-1} e^{-U_{eff}/T}, \quad (2)$$

with base frequency ${\tau_0}^{-1}$ and Orbach energy barrier U_{eff}.

Both models describe the almost constant inverse relaxation times up to approximately 10 K *via* a QTM process. The steeply increasing inverse relaxation times above 10 K can be explained by a Raman or, alternatively, also by an Orbach process. Table 1 lists the obtained spin–lattice relaxation parameters for models (1) and (2). The authors of this work want to emphasize that the average refined Raman temperature exponent n = 7 of model (1) is in the typical range expected for 'real' Raman relaxation processes from about 7 to 9 in contrast to many n values published for similar compounds (see Table S1†) that are much smaller. It should also be mentioned

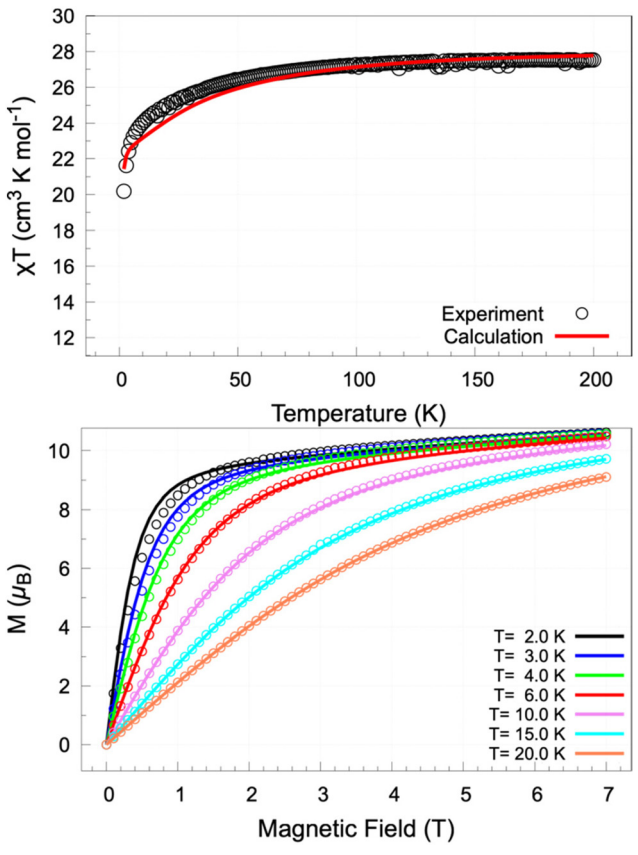

Fig. 2 Plots of $\chi_M T$ *vs.* T (top) under an applied DC field of 1 kOe from 2–220 K and field-dependent magnetization (bottom) for complex **1** at 2, 3, 4, 6, 10, 15 and 20 K under a DC field of up to 70 kOe. Comparison between measured and calculated molar magnetic susceptibility and magnetization at low temperature for **1** uses the magnetic interaction parameter derived from BS-DFT calculations. Magnetic dipole–dipole interaction was also considered. Circles and lines represent the experimental data points and fittings, respectively.

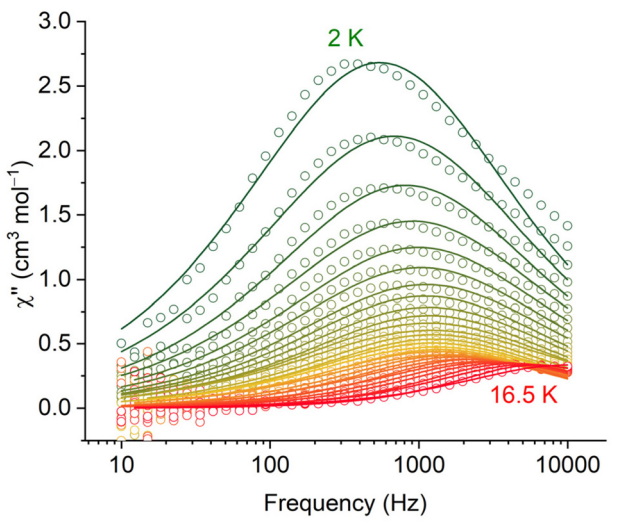

Fig. 3 Out-of-phase χ'' *vs.* ac excitation frequency for **1** under zero applied dc field from 2 to 16.5 K. Circles represent experimental data points. Solid lines represent fits to the data, as described in the main text.

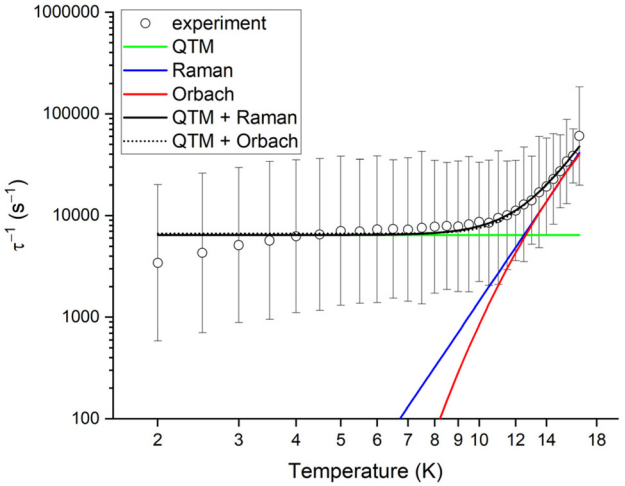

Fig. 4 Inverse relaxation rates *vs.* temperature extracted from ac susceptibility measurements for complex **1**. A fit to the experimental data is done using a 'QTM + Raman' model (eqn (1)) or, with equal quality, using a 'QTM + Orbach' model (eqn (2)).

here that the relatively large standard deviations obtained for the parameters listed are the result of the uncertainty estimates in magnetic relaxation times extracted from AC experiments and a consequent consideration of these by proper data evaluation.[27a]

For each temperature, the curve was fitted according to the generalized Debye model with α values (distribution of relaxation times) ranging from about 0.09 to 0.38, showing the broader distribution of the relaxation times and corresponding adiabatic and isothermal susceptibilities (Table S2†).

The energy barriers and relaxation times of complexes **A**–**H** have been estimated from AC susceptibility measurements (Table S1†).[21,22,29] However, the authors did not take into account the uncertainty of the relaxation times. It has been suggested by other authors that the uncertainty in AC magnetometry must be considered for valid comparisons with known SMMs.[27] Complexes **B**–**H** show relaxation in zero-field with QTM at low temperatures and, when a field is applied, QTM is efficiently suppressed.[21f,22b,29a–c] With a zero DC field, the magnetization of chain-like complex **A** relaxes more slowly than the magnetization in its comparable dimers due to the inefficiency of the QTM process. The uncertainty in the relaxation times of **A** can be tiny since the distribution of relaxation times in **A** is relatively narrow (0.03–0.08). The energy barriers of the SMMs **A**, **B** and **C** are 97.6, 37.9 and 48.7 K, respectively, which are relatively less than those of **1** and all other related complexes **D**, **E**, **F**, **G** and **H**.[21f,22b,29a–c] The inorganic core of complex **F** slightly resembles that of **1** having two Cl–K–Cl bridges, the difference being the type of ligand. The *ab initio* calculation of **F** shows that the magnetic moment relaxes through the $|+7/2\rangle$ to $|-7/2\rangle$ Kramers doublet with the energy barriers of 832–943 cm^{-1} for all four Dy^{3+} individual ions. This is also evident from the experimental energy barrier (1285 K ~ 893 cm^{-1}) extracted from the ac susceptibility measurements, while for complex **1**, *ab initio* calculations show that the magnetic moment relaxes through the $|+11/2\rangle$ to $|-11/2\rangle$ Kramers doublet in **1** with the energy barrier of 133/137 cm^{-1} for a single Dy^{3+} ion. At the same time, fitting the relaxation times within the error bars gives an energy barrier of U_{eff} = 100(70) K (Table 1). The larger standard deviation accounted for the significantly broader distribution of the relaxation times with α in the range of 0.09 to 0.38.[27] Complexes **D** to **H** display very slow relaxation having a high magnetization reversal barrier, as shown in Table S1.† The relaxation process parameters for the Raman process of complex **1** are in the range of the reported parameters for the other Cp–Dy SMMs shown in Table S1.†

Ab initio results

Data listed in Table 2 show that the magnitude of the ground state g_Z value (≈ 18.8 in Model 1 *vs.* 19.8 in Model 2)[13,21,22] is somewhat lower than that in many other performant Dy-based single-molecule magnets.[29] At the same time, the low-lying excited Kramers doublets are not that high in energy. The same trend is noticed from the total splitting of the ground J = 15/2 of Dy^{III}, which is significantly smaller than that of other top single-molecule magnets. This is a clear sign that the axiality of the crystal field is not that large. The main reason for the decreased crystal field splitting of the $[Dy(Cp)_2]$ unit is the destructive role played by the two Cl ligand ions, which act towards increasing the equatorial component of the crystal field, thus making the effect of the axial component less pronounced. The destructive role of the Cl ions also increases the steric pressure on the Cp ligands, making the angle between the centroids of the Cp ligands and Dy site smaller compared to that with $[Dy(Cp)_2]$ alone. These structural changes lead to significant changes in the electronic structure of the two Dy sites in **1**, as shown in Table 2 and Fig. 5, revealing the local (on-site) blocking barriers of individual Dy.

It is noticed that in both cases, the magnetization reversal barriers close at KD3. The tunneling at KD1 and KD2 is suppressed, given their near collinearity with each other (for both Dy sites), while the main g_Z axis of KD3 is nearly perpendicular to them (Fig. 5). This fact brings about a large matrix element of the transition magnetic moment between KD2 and KD3, leading to significant tunneling probability.

The magnetic exchange between the two Dy sites was evaluated using two approaches. The first approach consisted of applying the Lines model,[40] as implemented in POLY_ANISO, and fitting it to the available experimental data. The second method used ORCA software[41] to estimate the magnetic exchange from broken-symmetry DFT calculations. Both approaches give very small values of the magnetic exchange while giving a reasonable description of the measured magnetism. The comparison between measured and calculated magnetic susceptibility and magnetization of **1** are shown in Fig. 2. Given the relatively weak magnetic exchange, the exchange splitting is only −0.15 cm^{-1}, which means that the two exchange doublets arising from the coupling between two local Kramers doublets are thermally almost equally populated even at the lowest temperature used for current magnetic measurements.

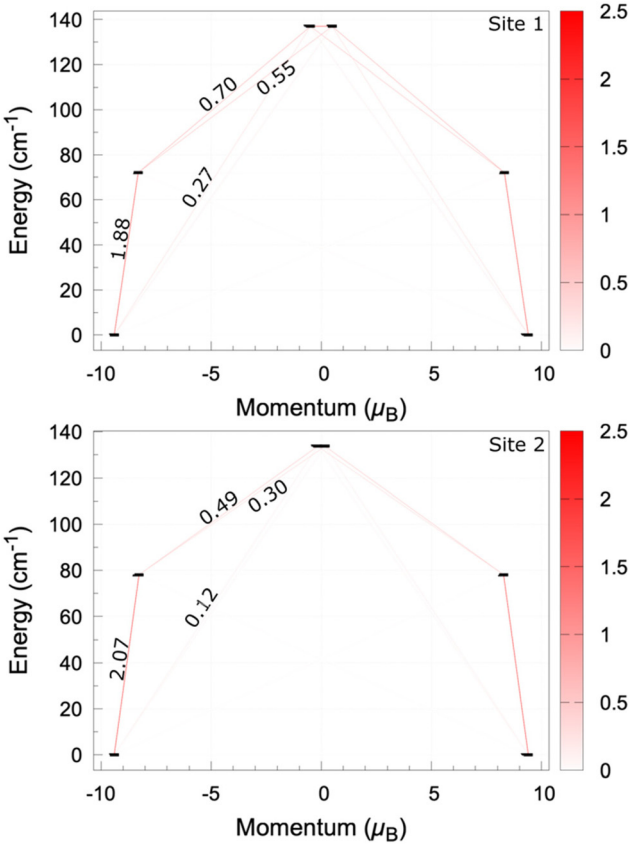

Fig. 5 Magnetization blocking barriers for individual Dy site. Note that the barriers for both sites close at KD3. The average values of the transition magnetic moments connecting the individual states are depicted with red lines, where the color intensity is proportional to the magnitude of the average transition magnetic moment. Both magnetic exchange and dipole–dipole interactions were considered.

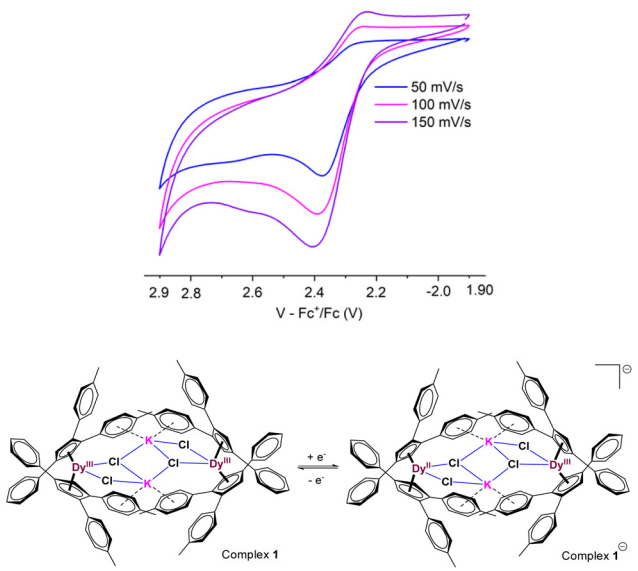

Fig. 6 CV of the complex $[(Cp^{Ar3})_4Dy^{III}_2Cl_4K_2]$ (**1**)in THF containing 0.1 M tetrabutylammonium hexafluorophosphate, employing silver as a reference electrode, glassy carbon as a working electrode and platinum as the counter electrode.

Redox properties

The CV measurements (Fig. 6) show that $[(Cp^{Ar3})_4Dy^{III}_2Cl_4K_2]$ (**1**) can undergo one-electron quasi-reversible reduction below −2.31 V in THF, suggesting the formation of $[(Cp^{Ar3})_4Dy^{II}Dy^{III}Cl_4K_2]^-$ ($\mathbf{1}^-$).

The second reduction process below −2.50 V is not reversible. $(C_5{}^iPr_5)_2Dy(II)$ was previously isolated by Long *et al. via* the reduction of its Dy(III) analogue.[28c]

Conclusions

We have investigated the dynamic magnetic properties of two weakly coupled (−0.15 cm^{-1}) Dy-metallocenes *via* a K_2Cl_4 bridge having a Dy–Dy separation of 8.23 Å. The coordination geometries of two Dy(III) centers are slightly different. This complex displays slow relaxation of magnetization below 17 K *via* KD3 energy levels (136.9/133.7 cm^{-1}) with the suppression of quantum tunneling of magnetizations of KD1 and KD2 energy levels due to the collinearity of each other, which has been concluded from CASSCF multi-reference calculations. A large matrix element of the transition magnetic moment between KD2 and KD3 might have assisted zero-field quantum tunneling. The Cole–Cole fit of the AC susceptibility plots shows a wider relaxation regime, which is also inferred by parameters with sizeable standard deviations from the fitting of the temperature-dependent relaxation time by Orbach and Raman processes. The significant structural distortion at Dy sites by two coordinating chloride ions led to a lowering of the axial anisotropic energy barrier of magnetization reorientation. The larger functional groups at the Cp-ring may have prevented the QTM process *via* intermolecular interactions.

Conflicts of interest

There are no conflicts to declare.

Acknowledgements

L.U. acknowledges the financial support of the research projects A-800079-00-00 and A-8000017-00-00 of the National University of Singapore. Ab initio calculations were done on the ASPIRE-1 cluster (www.nscc.sg) under projects 11001278 and 51000267. The computational resources of the HPC-NUS are gratefully acknowledged. KCM thanks SERB for ECR grant, ECR/2016/000890.

References

1 *The rare earth elements: fundamental and applications*, ed. D. A. Atwood, University of Kentucky, Lexington, KY, USA, 2012.

2 *Functional Hybrids Materials*, ed. P. Gomez-Romero and C. Sanchez, Wiley-VCH, Verlag GmbH & Co KGaA, Weinheim, Germany, 2004.
3 (*a*) D. Gatteschi, R. Sessoli and J. Villain, *Molecular nanomagnets*, Oxford University Press, Oxford, UK, 2006; (*b*) L. Thomas, F. Lionti, R. Ballou, D. Gatteschi, R. Sessoli and B. Barbara, *Nature*, 1996, **383**, 145; (*c*) T. G. Ashebr, H. Li, X. Ying, X. L. Li, C. Zhao, S. Liu and J. Tang, *ACS Mater. Lett.*, 2022, **4**, 307; D. N. Woodruff, R. E. P. Winpenny and R. A. Layfield, *Chem. Rev.*, 2013, **113**, 5110.
4 (*a*) L. D. Carlos, R. A. S. Ferreira, V. D. Z. Bermudez, B. J. Lopez and P. Escribano, *Chem. Soc. Rev.*, 2011, **40**, 536; (*b*) H. Schumann, J. A. M. Marktscheffel and L. Esser, *Chem. Rev.*, 1995, **95**, 865; (*c*) A. Z. Lekuona, J. M. Seco and E. Colacio, *Coord. Chem. Rev.*, 2021, **441**, 213984.
5 G. K. Veits and J. R. D. Alaniz, *Tetrahedron*, 2012, **68**, 2015.
6 R. Sessoli, H. L. Tsai, A. R. Schake, S. Wang, J. B. Vincent, K. Foiling, D. Gatteschi, G. Christou and D. N. Hendrickson, *J. Am. Chem. Soc.*, 1993, **115**, 1804.
7 (*a*) F. S. Guo, B. M. Day, Y. C. Chen, M. L. Tong, A. Mansikkamaki and R. A. Layfield, *Science*, 2018, **362**, 1400; (*b*) J. P. Durrant, B. M. Dey, J. Tang, A. Mansikkamaki and R. A. Layfield, *Angew. Chem., Int. Ed.*, 2022, **61**, e202200525; (*c*) J. M. Zadrozny, M. Nippe and J. R. Long, *J. Am. Chem. Soc.*, 2012, **134**, 18546–18549.
8 (*a*) F. S. Guo, B. M. Day, Y. C. Chen, M. L. Tong, A. M. Ki and R. A. Layfield, *Angew. Chem., Int. Ed.*, 2017, **56**, 11445; (*b*) C. A. Gould, K. R. McClain, D. Reta, J. G. C. Kragskow, D. A. Marchiori, E. Lachman, E. S. Choi, J. G. Analytis, R. D. Britt, N. F. Chilton, B. G. Harvey and J. R. Long, *Science*, 2022, **375**, 198.
9 C. A. P. Goodwin, F. Ortu, D. Reta, N. F. Chilton and D. P. Mills, *Nature*, 2017, **548**, 439.
10 (*a*) T. J. Kealy and P. L. Pauson, *Nature*, 1951, **168**, 1039; (*b*) S. A. Miller, J. A. Tebboth and J. F. Tremaine, *J. Chem. Soc.*, 1952, 632.
11 J. M. Birmingham and G. Wilkinson, *J. Am. Chem. Soc.*, 1956, **78**, 42.
12 F. T. Edelmann, *Coord. Chem. Rev.*, 2018, **370**, 129.
13 (*a*) B. M. Day, F. S. Guo and R. A. Layfield, *Acc. Chem. Res.*, 2018, **51**, 1880; (*b*) S. Lauk and A. Schafer, *Eur. J. Inorg. Chem.*, 2021, **48**, 5026.
14 (*a*) K. L. M. Harriman, D. Errulat and M. Murugesu, *Trends Chem.*, 2019, **1**, 425; (*b*) T. Pugh, F. Tuna, L. Ungur, D. Collison, E. J. L. McInnes, L. F. Chibotaru and R. A. Layfield, *Nat. Commun.*, 2015, **6**, 7492; (*c*) Y. S. Meng, Y. Q. Zhang, Z. M. Wang, B. W. Wang and S. Gao, *Chem. – Eur. J.*, 2016, **22**, 12724; (*d*) C. Gao, A. Genoni, S. Gao, S. Jiang, A. Soncini and J. Overgaard, *Nat. Chem.*, 2020, **12**, 213; (*e*) M. Briganti, E. Lucaccini, L. Chelazzi, S. Ciattini, L. Sorace, R. Sessoli, F. Totti and M. Perfetti, *J. Am. Chem. Soc.*, 2021, **143**, 8108.
15 (*a*) J. H. Jia, Q. W. Li, Y. C. Chen, J. L. Liu and M. L. Tong, *Coord. Chem. Rev.*, 2019, **378**, 365; (*b*) F. Pointillart, J. Jung, R. B. Pache, B. L. Guennic, V. Dorcet, S. Golhen, O. Cador, O. Maury, Y. Guyot, S. Decurtins, S. X. Liu and L. Ouahab, *Inorg. Chem.*, 2015, **54**, 5384; (*c*) D. Zeng, M. Ren, S. S. Bao, L. Li and L. M. Zheng, *Chem. Commun.*, 2014, **50**, 8356; (*d*) X. Yi, K. Bernot, F. Pointillart, G. Poneti, G. Calvez, C. Daiguebonne, O. Guillou and R. Sessoli, *Chem. – Eur. J.*, 2012, **18**, 11379; (*e*) J. Long, R. Vallat, R. A. S. Ferreira, L. D. Carlos, F. A. A. Paz, Y. Guari and J. Larionova, *Chem. Commun.*, 2012, **48**, 9974; (*f*) A. N. Kulakova, K. Nigoghossian, G. Felix, V. N. Khrustalev, E. S. Shubina, J. Long, Y. Guari, L. D. Carlos, A. N. Bilyachenko and J. Larionova, *Eur. J. Inorg. Chem.*, 2021, **18**, 2696; (*g*) R. Marin, G. Brunet and M. Murugesu, *Angew. Chem., Int. Ed.*, 2021, **60**, 1728.
16 (*a*) S. Lumetti, A. Candini, C. Godfrin, F. Balestro, W. Wernsdorfer, S. Klyatskaya, M. Ruben and M. Affonte, *Dalton Trans.*, 2016, **45**, 16570; (*b*) F. D. Natterer, K. Yang, W. Paul, P. Willke, T. Choi, T. Greber, A. J. Heinrich and C. P. Lutz, *Nature*, 2017, **543**, 226; (*c*) S. Sanvito, *Chem. Soc. Rev.*, 2011, **40**, 3336.
17 (*a*) R. E. P. Winpenny, *Angew. Chem., Int. Ed.*, 2008, **47**, 7992; (*b*) M. Affronte, *J. Mater. Chem.*, 2009, **19**, 1731.
18 (*a*) A. D. B. Dias, *Dalton Trans.*, 2007, 2229; (*b*) J. Kido and Y. Okamoto, *Chem. Rev.*, 2002, **102**, 2357.
19 (*a*) S. Pandya, J. Yu and D. Parker, *Dalton Trans.*, 2006, **23**, 2757; (*b*) H. Tsukube and S. Shinoda, *Chem. Rev.*, 2002, **102**, 2389.
20 (*a*) D. A. Bardonov, P. D. Komarov, V. I. Ovchinnikova, L. N. Puntus, M. E. Minyaev, I. E. Nifantev, K. A. Lyssenko, V. M. Korshunov, I. V. Taidakov and D. M. Roitershtein, *Organometallics*, 2021, **40**, 1235; (*b*) D. M. Roitershtein, L. N. Puntus, A. A. Vinogradov, K. A. Lyssenko, M. E. Minyaev, M. D. Dobrokhodov, I. V. Taidakov, E. A. Varaksina, A. V. Churakov and I. E. Nifantev, *Inorg. Chem.*, 2018, **57**, 10199; (*c*) R. P. Kelly, T. D. M. Bell, R. P. Cox, D. P. Daniels, G. B. Deacon, F. Jaroschik, P. C. Junk, X. F. L. Goff, G. Lemercier, A. Martinez, J. Wang and D. Werner, *Organometallics*, 2015, **34**, 5624; (*d*) A. Strasser and A. Vogler, *Chem. Phys. Lett.*, 2003, **379**, 287.
21 (*a*) R. A. Layfield, J. J. W. McDouall, S. A. Sulway, F. Tuna, D. Collison and R. E. P. Winpenny, *Chem. – Eur. J.*, 2010, **16**, 4442; (*b*) F. Tuna, C. A. Smith, M. Bodensteiner, L. Ungur, L. F. Chibotaru, E. J. L. McInnes, R. E. P. Winpenny, D. Collison and R. A. Layfield, *Angew. Chem., Int. Ed.*, 2012, **51**, 6976; (*c*) R. Grindell, B. M. Day, F. S. Guo, T. Pugh and R. A. Layfield, *Chem. Commun.*, 2017, **53**, 9990; (*d*) F. S. Guo and R. A. Layfield, *Chem. Commun.*, 2017, **53**, 3130; (*e*) T. Pugh, N. F. Chilton and R. A. Layfield, *Angew. Chem., Int. Ed.*, 2016, **55**, 11082; (*f*) S. A. Sulway, R. A. Layfield, F. Tuna, W. Wernsdorfer and R. E. P. Winpenny, *Chem. Commun.*, 2012, **48**, 1508.
22 (*a*) P. Evans, D. Reta, C. A. P. Goodwin, F. Ortu, N. F. Chilton and D. P. Mills, *Chem. Commun.*, 2020, **56**, 5677; (*b*) D. Errulat, B. Gabidullin, A. Mansikkamaki and M. Murugesu, *Chem. Commun.*, 2020, **56**, 5937; (*c*) M. He, F. S. Guo, J. Tang, A. Mansikkamaki and R. A. Layfield,

Chem. Sci., 2020, **11**, 5745; (*d*) C. P. Burns, B. O. Wilkins, C. M. Dickie, T. P. Latendresse, L. Vernier, K. R. Vignesh, N. S. Bhuvanesh and M. Nippe, *Chem. Commun.*, 2017, **53**, 8419.

23 (*a*) S. Demir, M. I. Gonzalez, L. E. Darago, W. J. Evans and J. R. Long, *Nat. Commun.*, 2017, **8**, 2144; (*b*) C. A. Gould, E. Mu, V. Vieru, L. E. Darago, K. Chakarawet, M. I. Gonzalez, S. Demir and J. R. Long, *J. Am. Chem. Soc.*, 2020, **142**, 21197; (*c*) S. Demir, M. Nippe, M. I. Gonzalez and J. R. Long, *Chem. Sci.*, 2014, **5**, 4701; (*d*) S. Demir, J. M. Zadrozny, M. Nippe and J. R. Long, *J. Am. Chem. Soc.*, 2012, **134**, 18546; (*e*) E. Castellanos, F. Benner and S. Demir, *Inorg. Chem. Front.*, 2022, **9**, 1325; (*f*) S. Demir, I. R. Jeon, J. R. Long and T. D. Harris, *Coord. Chem. Rev.*, 2015, **289**, 149; (*g*) F. Benner and S. Demir, *Chem. Sci.*, 2022, **13**, 5818–5829; (*h*) E. R. Pugliese, F. Benner, E. Castellanos, F. Delano IV and S. Demir, *Inorg. Chem.*, 2022, **61**, 2444–2454.

24 S. Arumugam, P. G. Reddy, M. Francis, A. Kulkarni, S. Roy and K. C. Mondal, *RSC Adv.*, 2020, **10**, 39366.

25 (*a*) M. Guo, Y. Wang, J. Wu, L. Zhao and J. Tang, *Dalton Trans.*, 2017, **46**, 564–570; (*b*) S. S. Liu, Y. S. Meng, Y. Q. Zhang, Z. S. Meng, K. Lang, Z. L. Zhu, C. F. Shang, B. W. Wang and S. Gao, *Inorg. Chem.*, 2017, **56**, 7320.

26 M. Gregson, N. F. Chilton, A. M. Ariciu, F. Tuna, I. F. Crowe, W. Lewis, A. J. Blake, D. Collison, E. J. L. McInnes, R. E. P. Winpenny and S. T. Liddle, *Chem. Sci.*, 2016, **7**, 155.

27 (*a*) D. Reta and N. F. Chilton, *Phys. Chem. Chem. Phys.*, 2019, **21**, 23567; (*b*) N. F. Chilton, R. P. Anderson, L. D. Turner, A. Soncini and K. S. Murray, *J. Comput. Chem.*, 2013, **34**, 1164–1175.

28 (*a*) M. He, F.-S. Guo, J. Tang, A. Mansikkamäki and R. A. Layfield, *Chem. Commun.*, 2021, **57**, 6396–6399; (*b*) F.-S. Guo, M. He, G.-Z. Huang, S. R. Giblin, D. Billington, F. W. Heinemann, M.-L. Tong, A. Mansikkamäki and R. A. Layfield, *Inorg. Chem.*, 2022, **61**, 6017–6025; (*c*) C. A. Gould, K. R. McClain, J. M. Yu, T. J. Groshens, F. Furche, B. G. Harvey and J. R. Long, *J. Am. Chem. Soc.*, 2019, **141**, 12967–12973; (*d*) T. Pugh, F. Tuna, L. Ungur, D. Collison, E. J. L. McInnes, L. F. Chibotaru and R. A. Layfield, *Nat. Commun.*, 2015, **6**, 7492.

29 (*a*) S. Demir, M. D. Boshart, J. F. Corbey, D. H. Woen, M. I. Gonzalez, J. W. Ziller, K. R. Meihaus, J. R. Long and W. J. Evans, *Inorg. Chem.*, 2017, **56**, 15049–15056; (*b*) C. Wang, R. Sun, Y. Chen, B.-W. Wang, Z.-M. Wang and S. Gao, *CCS Chem.*, 2020, **2**, 362–368; (*c*) S. Demir, J. M. Zadrozny and J. R. Long, *Chem. – Eur. J.*, 2014, **31**, 9524–9529; (*d*) S. Demir, M. I. Gonzalez, L. E. Darago, W. J. Evans and J. R. Long, *Nat. Commun.*, 2017, **8**, 2144; (*e*) H.-S. Wang, P.-F. Zhou, J. Wang, Q.-Q. Long, Z. Hu, Y. Chen, J. Li, Y. Song and Y.-Q. Zhang, *Inorg. Chem.*, 2021, **60**, 18739–18752; (*f*) H. Tian, B.-L. Wang, J. Lu, H.-T. Liu, J. Su, D. Li and J. Dou, *Chem. Commun.*, 2018, **54**, 12105–12108.

30 I. Fdez Galvan, M. Vacher, A. Alavi, C. Angeli, F. Aquilante, J. Autschbach, J. J. Bao, S. I. Bokarev, N. A. Bogdanov, R. K. Carlson, L. F. Chibotaru, J. Creutzberg, N. Dattani, M. G. Delcey, S. S. Dong, A. Dreuw, L. Freitag, L. M. Frutos, L. Gagliardi, F. Gendron, A. Giussani, L. Gonzalez, G. Grell, M. Guo, C. E. Hoyer, M. Johansson, S. Keller, S. Knecht, G. Kovacevic, E. Kallman, G. Li Manni, M. Lundberg, Y. Ma, S. Mai, J. P. Malhado, P. A. Malmqvist, P. Marquetand, S. A. Mewes, J. Norell, M. Olivucci, M. Oppel, Q. M. Phung, K. Pierloot, F. Plasser, M. Reiher, A. M. Sand, I. Schapiro, P. Sharma, C. J. Stein, L. K. Sorensen, D. G. Truhlar, M. Ugandi, L. Ungur, A. Valentini, S. Vancoillie, V. Veryazov, O. Weser, T. A. Wesolowski, P.-O. Widmark, S. Wouters, A. Zech, J. P. Zobel and R. Lindh, *J. Chem. Theory Comput.*, 2019, **15**, 5925–5964.

31 F. Aquilante, J. Autschbach, R. K. Carlson, L. F. Chibotaru, M. G. Delcey, L. De Vico, I. Fdez Galvan, N. Ferre, L. M. Frutos, L. Gagliardi, M. Garavelli, A. Giussani, C. E. Hoyer, G. Li Manni, H. Lischka, D. Ma, P. A. Malmqvist, T. Muller, A. Nenov, M. Olivucci, T. B. Pedersen, D. Peng, F. Plasser, B. Pritchard, M. Reiher, I. Rivalta, I. Schapiro, J. Segarra-Marti, M. Stenrup, D. G. Truhlar, L. Ungur, A. Valentini, S. Vancoillie, V. Veryazov, V. P. Vysotskiy, O. Weingart, F. Zapata and R. Lindh, *J. Comput. Chem.*, 2016, **37**, 506–541.

32 B. O. Roos, R. Lindh, P.-A. Malmqvist, V. Veryazov, P.-O. Widmark and A. C. Borin, *J. Phys. Chem. A*, 2008, **112**, 11431–11435.

33 (*a*) B. O. Roos, P. R. Taylor and P. E. M. Siegbahn, *Chem. Phys.*, 1980, **48**, 157–173; (*b*) P. E. M. Siegbahn, J. Almlöf, A. Heiberg and B. O. Roos, *J. Chem. Phys.*, 1981, **74**, 2384–2396.

34 P. A. Malmqvist, B. O. Roos and B. Schimmelpfennig, *Chem. Phys. Lett.*, 2002, **357**, 230–240.

35 L. F. Chibotaru and L. Ungur, *J. Chem. Phys.*, 2012, **137**, 064112.

36 L. F. Chibotaru, Ab Initio Methodology for Pseudospin Hamiltonians of Anisotropic Magnetic Complexes, in *Advances in Chemical Physics*, ed. S. A. Rice and A. R. Dinner, Wiley, 2013, vol. 153, pp. 397–519.

37 L. Ungur and L. F. Chibotaru, Computational Modelling of the Magnetic Properties of Lanthanide Compounds, in *Lanthanides and Actinides in Molecular Magnetism*, ed. R. A. Layfield and M. Murugesu, Wiley-VCH, 2015, pp. 153–184.

38 L. Chibotaru, *Struct. Bonding*, 2014, **164**, 185–230.

39 L. F. Chibotaru and L. Ungur, *The computer programs SINGLE_ANISO and POLY_ANISO*, University of Leuven, 2006.

40 (*a*) L. F. Chibotaru, L. Ungur and A. Soncini, *Angew. Chem., Int. Ed.*, 2008, **47**, 4126–4129; (*b*) M. E. Lines, *J. Chem. Phys.*, 1971, **55**, 2977–2984.

41 F. Neese, Software update: The ORCA program system—Version 5.0, *Wiley Interdiscip. Rev.: Comput. Mol. Sci.*, 2022, **12**, e1606.